Publishing Excellence Inspiring Progress
ARISTON PUBLICATIONS
Energy & Environment Advances
ISSN: 3066-5728 https://aristonpubs.com/energy-environment-advances https://doi.org/10.69626/eea.2025.0032

RESEARCH ARTICLE

Biochar Produced from Dead Pine Needles to Produce Biochar/CuO and Biochar/CuO/BaO for Water and Biomedical Remediation

Shweta Kaushal [1,2], Subhash Chand [1,2], Anshul Kumar [1,2], Neha Sharma [1,2], Deepak Sharma [1,2], Dikender Kumar [1,2], Kuldeep Kumar [1,2,*]

ABSTRACT: The sustainable utilization of biomass waste for environmental applications has gained significant interest in recent years. This study explores the synthesis of biochar-based metal oxide composites, Biochar/CuO and Biochar/CuO/BaO, using biochar derived from the pyrolysis of dead pine needles, an abundant forest residue. Copper oxide (CuO) and barium oxide (BaO) were integrated into the biochar matrix to enhance its photocatalytic and antimicrobial properties. The prepared composites were characterized using X-ray diffraction (XRD), ultraviolet-visible spectroscopy (UV-Vis), Fourier-transform infrared spectroscopy (FTIR), and scanning electron microscopy (SEM) to confirm their crystallinity, optical behavior, functional groups, morphology, and elemental composition. The Biochar/CuO and Biochar/CuO/BaO composites exhibited superior photocatalytic activity, achieving significant degradation of methylene blue dye under visible light irradiation, attributed to the synergistic effects of biochar's high surface area and the metal oxides' semiconductor properties. Additionally, the composites demonstrated potent antibacterial activity against *Enterococcus faecalis*, a gram positive bacteria, owing to the generation of reactive oxygen species. These findings highlight the potential of pine needle-derived biochar-metal oxide composites as cost-effective, eco-friendly materials for dye degradation and microbial control. This work contributes to the valorization of forest waste and the development of multifunctional nanomaterials for environmental remediation and public health applications.

Keywords: Pine Needle Waste, Metal Oxide Composites, Photocatalysis, Antimicrobial Activity, Sustainable Materials

Received: 01 October 2024; Revised: 17 November 2024; Accepted: 28 December 2024; Published Online: 19 January 2025

1. INTRODUCTION

The rapid industrialization and increasing urban population have led to the widespread release of synthetic dyes and pathogenic microbes into aquatic ecosystems, resulting in severe environmental and public health challenges [1].The increasing environmental issues associated to water pollution from synthetic dyes and microbial pathogens have prompted the development of sustainable and effective remedial methods. Among the various pollutants, synthetic dyes such as methylene blue (MB), a common cationic dye extensively used in the textile and paper industries, are of particular concern. MB is highly stable, difficult to degrade biologically, and potentially toxic to aquatic life and humans [2]. Moreover, the rise of antibiotic-resistant bacteria such as *Enterococcus faecalis* has intensified the need for effective antibacterial agents, especially in the context of waterborne diseases and biofilm-related infections [3].

Biochar, produced through the pyrolysis of biomass, has become an environmentally sustainable and economically viable material owing to its elevated surface area, porosity, and functional groups. It makes it suitable for diverse environmental applications [4,5]. Methylene Blue is a widely used cationic synthetic dye in the textile and printing industries. It is notorious for its resilience and toxicity. It

[1] Department of Chemistry, Career Point University, Hamirpur, Himachal Pradesh, 176041, India.
[2] Center for Nano-Science and Technology, Career Point University, Hamirpur, Himachal Pradesh, 176041, India.

* Author to whom correspondence should be addressed: kuldeep.sharma.753@gmail.com (Kuldeep Kumar)

requires effective and environmentally sustainable remediation strategies [6]. The rise of microbial resistance to traditional antibiotics has increased the demand for innovative materials possessing antibacterial and antifungal capabilities to address pathogenic concerns [7]. In this context, biochar-based nanomaterials have emerged as promising multifunctional materials due to their cost effectiveness, environmental friendly nature, and tunable physicochemical properties [8].

Biochar derived from the pyrolysis of biomass due to its high surface area and porosity is promising material for wastewater treatment [9]. Dead pine needles offer a valuable feedstock for biochar production due to their abundance as forest waste. It not only solves waste management and reduces forest fires but also aligns to the ideas of a circular economy [10]. The adsorption capacity and efficacy of biochar generated from deceased pine needles can be markedly improved with the incorporation of metal oxide nanoparticles. It enhances the number of active sites and enhances photo-catalytic activities [8]. Copper oxide (CuO), a p-type semiconductor, is notably appealing due to its low bandgap. It is recognized for its photocatalytic efficacy in dye degradation and intrinsic antibacterial characteristics [11]. Furthermore, the incorporation of barium oxide into CuO/biochar systems could potentially modifies the composite's bandgap. It reduces electron-hole pair recombination and improves photocatalytic efficiency. This synergy improves the material's capacity to decay organic pollutants under light exposure and inhibit microbial growth.

In this study, a simple, one-step pyrolysis method was employed to synthesize biochar-based nanocomposites, Biochar/CuO and Biochar/CuO/BaO, using dead pine needles as the carbon precursor and copper and barium nitrates as metal sources. The process not only results in porous biochar but also enables uniform integration of metal oxide nanoparticles. This technique utilizes molten salt activation to concurrently create a porous biochar matrix and incorporate CuO and CuO/BaO nanoparticles, enhancing the material for the degradation of MB dye under visible light The practical applicability of these materials was then evaluated for two targeted purposes: (i) photocatalytic degradation of methylene blue dye under visible light, and (ii) antibacterial activity against *Enterococcus faecalis*, a Gram-positive opportunistic pathogen. The antibacterial testing was conducted using the Kirby-Bauer disc diffusion method at varying concentrations of the synthesized materials. This dual-purpose application aligns with the growing need for sustainable materials that address both environmental pollution and microbial contamination [12]. By integrating forest biomass valorization with nanomaterial synthesis, this research offers a sustainable route for producing multifunctional materials aimed at water purification and selective microbial inhibition. The findings demonstrate that CuO and BaO incorporation significantly enhances the photocatalytic and antibacterial capabilities of biochar, highlighting its potential as a dual-functional material for environmental remediation.

2. MATERIALS AND METHODS

2.1. Materials

Dead pine needles were collected from a forested area in Career Point University, Hamirpur. Copper nitrate ($Cu(NO_3)_2 \cdot 3H_2O$, ≥ 98%) and barium nitrate ($Ba(NO_3)_2$, ≥ 98%) were procured from Sigma-Aldrich. Methylene blue, used for potential testing, was purchased from Oxford, Dimethyl Sulfoxide, Mueller-Hinton Agar and Ciprofloxacin were procured form SRL, Bacterial Culture (Enterococcus faecalis, MTCC 429) Procured from Microbial Type Culture Collection and Gene Bank (MTCC)- Chandigarh. All chemicals were used as received without further purification.

2.2. Methods

Biochar and its composites (Biochar/CuO and Biochar/CuO/BaO) were synthesized via a facile one-step pyrolysis method under oxygen-limited conditions as shown by Thi luyen et al., (2023) [12], utilizing dead pine needles as the carbon precursor and metal nitrates as precursors for CuO and BaO. The dead pine needles were first washed with deionized (DI) water to remove surface impurities, dried at 100 °C for 24 hours, ground into a fine powder, and sieved through a mesh with a pore size of 0.154 mm. For the synthesis of biochar (BC), the dried pine needle powder was pyrolyzed without metal salts. For Biochar/CuO composites, copper nitrate ($Cu(NO_3)_2 \cdot 3H_2O$) was physically mixed with the pine needle powder. For Biochar/CuO/BaO composites, both copper nitrate and barium nitrate were mixed with the pine needle powder. Pyrolysis was performed in a muffle furnace with a heating rate of 10 °C min^{-1} under oxygen-limited conditions. The mixtures were placed in a porcelain cup with a lid and heated at temperatures of 700 °C for 2 hours. After pyrolysis, the furnace was cooled to room temperature naturally. The resulting samples were washed several times several times with DI water to remove unreacted salts and impurities, then dried at 60 °C for 24 hours.

2.3. Characterization

The morphological features and elemental composition of the biochar (BC), Biochar/CuO, and Biochar/CuO/BaO composites were investigated using field emission scanning electron microscopy (FE-SEM; Hitachi S4800) and transmission electron microscopy (TEM; JEM 1400 Flash). X-ray diffraction (XRD) patterns were obtained using an X-ray diffractometer (Bruker D2) to analyze the crystalline structure and crystallite size of the samples. The surface chemical functional groups present in the materials were examined by Fourier transform infrared spectroscopy (FTIR-4600 Jasco) in the wavenumber range of 400−4000 cm^{-1}. The absorbance properties and band gap energies of the samples were determined using UV-Visible spectroscopy. Elemental

composition was further confirmed by energy-dispersive X-ray spectroscopy (EDS) coupled with FE-SEM.

3. RESULTS AND DISCUSSION

3.1. XRD analysis

The X-ray diffraction (XRD) patterns of pristine biochar, Biochar/CuO, and Biochar/CuO/BaO composites were analyzed to investigate their crystallographic structures and the effects of metal oxide impregnation (Figure 1). The measurements were conducted using Cu Kα radiation (λ = 1.5406 Å) over a 2θ range of 10° to 80°, providing insights into the amorphous and crystalline phases present in these materials.

The XRD pattern of pristine biochar exhibits a predominantly amorphous structure, characterized by a broad, low-intensity diffraction hump centered around 20°–25° 2θ (d-spacing ≈ 3.5–4.5 Å), which is typical of disordered graphitic carbon derived from biomass pyrolysis [13]. Minor sharp peaks are observed, such as at approximately 10° 2θ (d ≈ 8.8 Å), which may indicate residual organic or mineral phases (e.g., potassium or calcium compounds) from the pine needle feedstock. The overall low crystallinity and absence of prominent mineral peaks (e.g., calcite at 29.4° or quartz at 26.6°) suggest a high carbon content with minimal ash-related crystalline impurities.

The incorporation of CuO into the biochar matrix significantly alters the XRD pattern. The pattern displays several sharp diffraction peaks superimposed on the amorphous carbon background. Notable peaks appear at approximately 35.5°, 38.7°, and 48.7° 2θ, which correspond to the (002), (111), and (202) planes of monoclinic CuO (JCPDS No. 48-1548) [14]. These peaks indicate the successful impregnation of crystalline CuO nanoparticles onto the biochar surface. The intensity of the amorphous carbon hump (20°–25° 2θ) is reduced compared to pristine biochar, suggesting partial disruption of the carbon structure or masking by the CuO phases.

The XRD pattern of the Biochar/CuO/BaO composite further evolves with the addition of BaO. In addition to the CuO peaks observed at 35.5°, 38.7°, and 48.7° 2θ, new diffraction peaks emerge, notably around 27.9°, 32.1°, and 46.5° 2θ. These peaks are consistent with the (100), (101), and (102) planes of hexagonal BaO (JCPDS No. 74-1227) or related barium compounds (e.g., $BaCO_3$) formed during synthesis [15]. The intensity of the CuO peaks appears enhanced, suggesting a synergistic effect where BaO may promote CuO crystallization or increase the loading of metal oxides. The amorphous carbon hump remains subdued, indicating that the metal oxide impregnation dominates the crystalline contribution, potentially due to higher pyrolysis temperatures or chemical interactions altering the carbon matrix. The presence of multiple sharp peaks also suggests a composite with a heterogeneous microstructure.

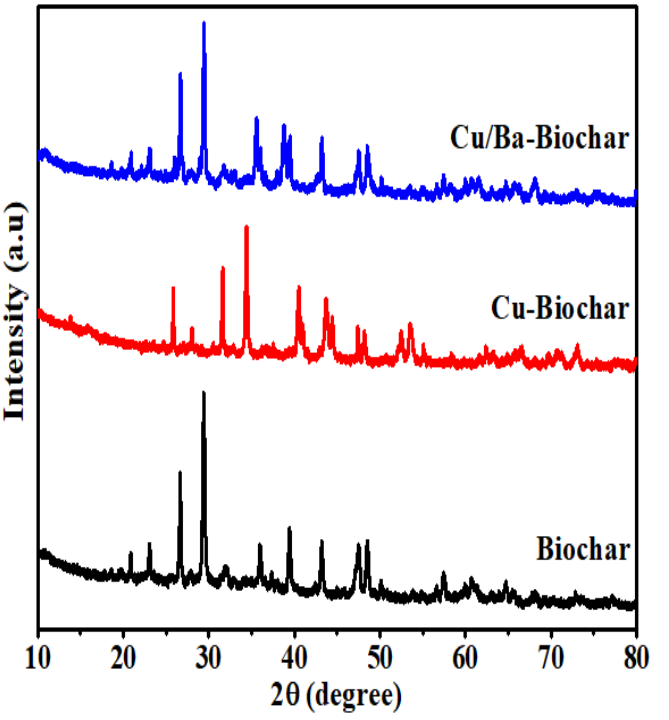

Fig. 1. XRD pattern of the Biochar, Cu-Biochar and Cu/Ba-Biochar samples.

The crystallite size and interplanar spacing were measured using the Scherer equation (eq. 1), and Braggs relation (eq. 2), respectively:

$$D = \frac{K*\lambda}{\beta*\cos\vartheta} \quad (1)$$

$$d = \frac{n*\lambda}{2*\sin\vartheta} \quad (2)$$

where D is the crystallite size, d is interplanar spacing, K is constant, β is FWHM of peak, θ is the angle of diffraction, and λ represents wavelength of the X-ray radiation. For the calculation of dislocation density and strain induced in biochar/CuO and biochar/CuO/BaO composites, formulas given in Eqs. (3), and (4) were used and results are expressed in tabular form as Table 1:

$$\delta = \frac{1}{D^2} \quad (3)$$

where D is the crystallite size.

$$\varepsilon = \frac{\beta \cos \vartheta}{4} \quad (4)$$

where β is the FWHM for most intense peak and θ is the Bragg's angle. The increase in dislocation density and strain in BC/CuO and BC/CuO/BaO signifies the existence of defects in composites.

Table 1. Structural parameters for the Biocahr, BC/CuO, and Biochar/CuO/BaO samples.

Samples	Crystallite size (D) (nm)	Interplanar spacing (d) (nm)	Dislocation density (δ) (nm^{-2})	Strain (ε)
Biochar	18.96	0.30	0.0028	0.0018
BC/CuO	15.18	0.25	0.0043	0.0022
BC/CuO/BaO	11.92	0.23	0.007	0.0029

3.2. FTIR analysis

Fourier Transform Infrared (FTIR) spectroscopy was used to analyze the functional groups in dead pine needles-derived biochar and its composites with copper oxide (CuO) and barium oxide (BaO) (Figure 2). The FTIR spectra have shown distinct differences in the chemical composition of the three materials across the wavenumber range of 4000 to 500 cm^{-1}. The spectrum of pure biochar showed characteristic peaks at 3701 cm^{-1}, 2369 cm^{-1}, 1414 cm^{-1}, 1025 cm^{-1}, 871 cm^{-1}, 579 cm^{-1}, and 571 cm^{-1}. The sharp peak at 3701 cm^{-1} indicates the presence of alcohols or phenols, while the peak at 2369 cm^{-1} may correspond to C=O stretching from carbonyl groups or atmospheric CO_2. The prominent peak at 1414 cm^{-1} suggests C=O stretching from carboxyl or ketone groups or aromatic C=C stretching.

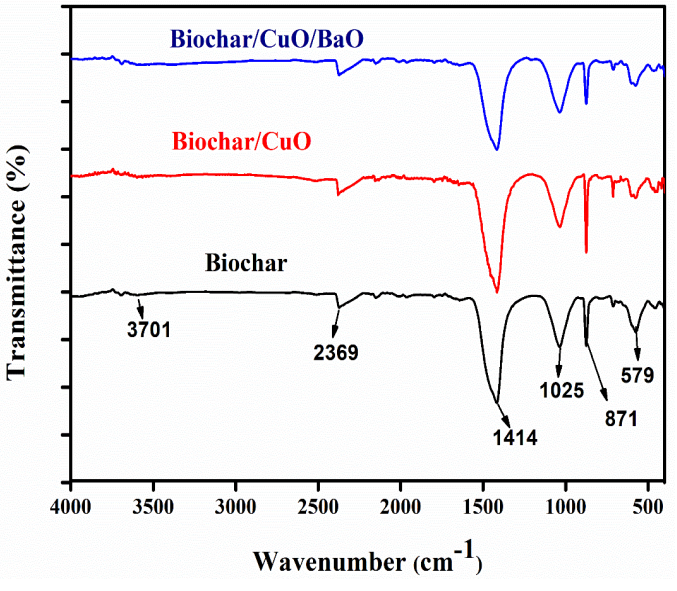

Fig. 2. FTIR spectra of the Biochar, Cu-Biochar and Cu/Ba-Biochar samples.

The smaller peaks at 871 cm^{-1}, 579 cm^{-1}, and 571 cm^{-1} in the fingerprint region indicate aromatic C-H bending or metal-oxygen bonds [16]. Incorporation of CuO into the biochar matrix (Biochar/CuO) modifies the spectrum, particularly in the fingerprint region below 1500 cm^{-1}. Peaks at 1414 cm^{-1}, 1025 cm^{-1}, 871 cm^{-1}, 579 cm^{-1}, and 571 cm^{-1} become more pronounced or shift, suggesting the formation of Cu-O bonds or interactions between CuO and the biochar's functional groups [17]. The addition of BaO to form Biochar/CuO/BaO results in a more complex spectrum, with enhanced peaks and new features, especially between 1500 cm^{-1} and 500 cm^{-1}. This indicates the incorporation of Ba-O bonds and possible synergistic effects between CuO and BaO, further altering the biochar surface chemistry [18].

3.3. UV-Visible analysis

Figures 3 (a-d) display UV–Vis absorbance spectra between 200 and 800 nm and Tauc plots for the synthesized biochar (BC), BC/CuO, and BC/CuO/BaO samples. The absorption spectrum of biochar exhibits a sharp peak in the UV region (200-250 nm) with minimal absorbance in the visible region (400-800 nm). The corresponding Tauc plot reveals an optical bandgap of 1.94 eV. This relatively high bandgap indicates that biochar behaves as a wide bandgap semiconductor, limiting its electronic transitions under visible light and aligning with the properties of carbonaceous materials [19]. Upon incorporation of CuO, the absorption spectrum of Cu-Biochar shows a slight extension into the visible region, with a less pronounced decline after the UV peak. The Tauc plot indicates a reduced bandgap of 1.63 eV. This decrease suggests that CuO introduces new energy states within the biochar's electronic structure, enabling electron transitions at lower energies and enhancing visible light absorption [20]. The Cu/Ba-Biochar composite, doped with both CuO and BaO, displays the highest absorbance, with a prominent UV peak and a significant tail extending into the visible region (up to 500-600 nm). Its Tauc plot yields the lowest bandgap of 1.3 eV among the three materials. This further reduction highlights the synergistic effect of CuO and BaO, which likely introduces additional defect states or modifies charge distribution, further facilitating low-energy electronic transitions [21].

3.4. SEM analysis

Figure 4 (a-c) exhibit Scanning electron microscopy (SEM) analysis of biochar, biochar/CuO, and biochar/CuO/BaO composites, revealing distinct structural transformations with the incorporation of CuO and BaO onto the biochar matrix. The pure biochar, exhibits a highly porous and irregular surface characterized by interconnected pores and rough, uneven particles.

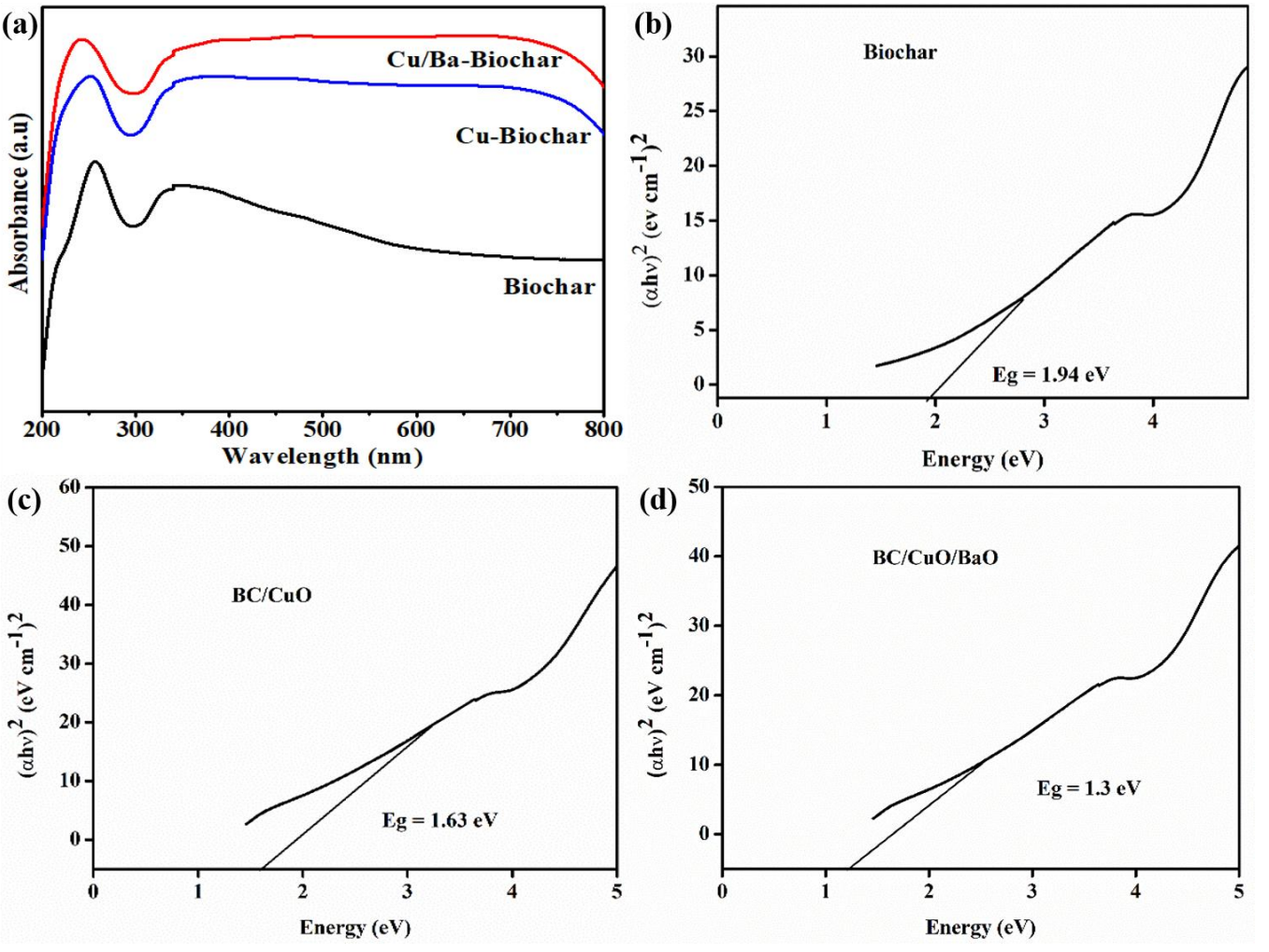

Fig. 3. (a) UV-Visible graph, and (b-d) Tauc-plots of the Biochar, Cu-Biochar and Cu/Ba-Biochar samples.

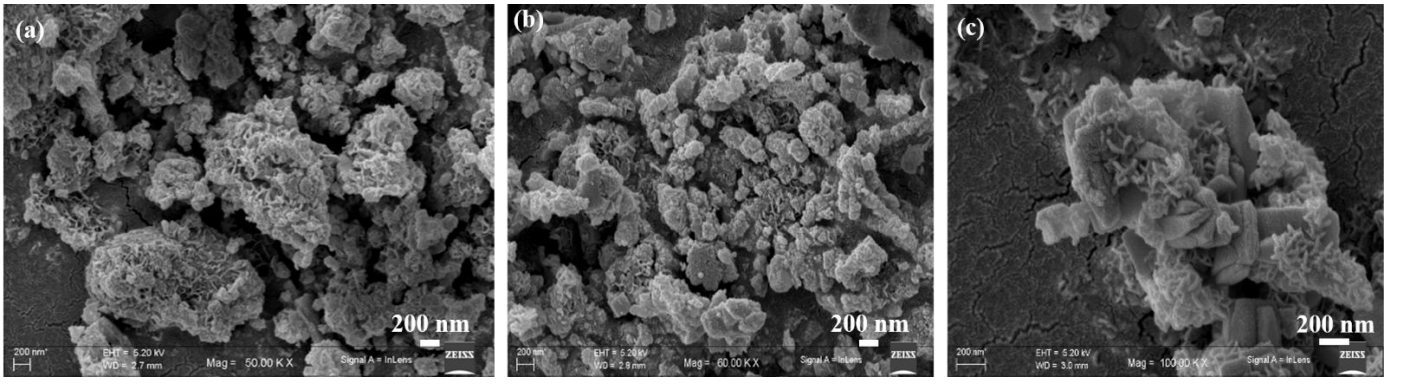

Fig. 4. (a-c) Typical SEM images of Biochar, Biochar/CuO and Biochar/CuO/BaO samples.

This sponge-like structure, typical of biochar derived from biomass pyrolysis, consists of agglomerated particles with varying sizes and shapes [22]. The biochar/CuO composite, shows a modified surface morphology. While retaining some porosity, the surface displays a denser aggregation of finer, more uniform particles, indicative of CuO nanoparticle deposition. This coating or impregnation effect results in a slightly smoother texture and reduced pore visibility in certain areas, suggesting partial filling by CuO [23]. The biochar/CuO/BaO composite, presents the most complex morphology. The addition of BaO induces the formation of pronounced, flower-like or crystalline structures protruding

unevenly across the surface. These features enhance surface roughness and establish a hierarchical architecture, while some regions preserve the underlying porous biochar framework, hinting at additional chemical interactions or phase formation [24].

3.5. Antibacterial activity

The antibacterial properties of biochar (BC), biochar impregnated with copper oxide (BC/CuO), and biochar impregnated with both copper oxide and barium oxide (BC/CuO/BaO) were assessed against *Enterococcus faecalis* (MTCC 429) using the Kirby-Bauer disc diffusion method [25]. Mueller-Hinton Agar (MHA) plates were inoculated with 100 µl of bacterial culture standardized to 0.5 McFarland (approximately 1.5×10^8 CFU/mL). Whatman No. 1 filter paper discs (5 mm) were impregnated with 10 µl of sample solutions at concentrations of 0, 50, 125, 250, 500, and 1000 µg/ml, prepared in dimethyl sulfoxide (DMSO) due to insolubility in ethanol. DMSO served as the negative control, and ciprofloxacin (3 µg/disc) was the positive control. After incubation at 37 °C for 24 hours, zones of inhibition (ZOI) were measured.

Table 2 provides a comprehensive breakdown of the ZOI values (in mm) for each material across the tested concentrations, alongside the controls. The data reveal a dose-dependent antibacterial effect: at 0 µg/ml, no inhibition was observed (0 mm), mirroring the negative control, whereas ciprofloxacin yielded a ZOI of 28–28.5 mm. At 50 µg/ml, BC showed a modest ZOI of 4 mm, while BC/CuO and BC/CuO/BaO exhibited significantly larger zones of 7.5 mm and 7.7 mm, respectively. At 1000 µg/ml, BC/CuO reached a ZOI of 11 mm, surpassing BC/CuO/BaO (10 mm) and BC (7 mm) as shown in Figure 5 and Figure 6.

The results highlight that impregnation with CuO particles significantly enhances the antibacterial efficacy of biochar. The CuO/biochar composites exhibit a larger specific surface, which contributes to their superior antibacterial performance. This suggests that the presence of biochar enhances the effectiveness of CuO nanoparticles in inhibiting bacterial growth [26]. Across all concentrations, BC/CuO consistently outperformed BC alone, with ZOI values increasing from 4 mm (BC) to 7.5 mm (BC/CuO) at 50 µg/ml and from 7 mm (BC) to 11 mm (BC/CuO) at 1000 µg/ml. This marked improvement underscores the critical role of CuO in boosting the material's antibacterial potency [27].

Table 2. ZOI values of BC, BC/CuO and BC/CuO/BaO against *Enterococcus faecalis.*

Dose (µg/ml)	BC (mm)	BC/CuO (mm)	BC/CuO/BaO (mm)
PC (ciprofloxacin)	28	28.5	28
0	0	0	0
50	4	7.5	7.7
125	6	7.5	8
250	6	7.5	8
500	7	10	9
1000	7	11	10

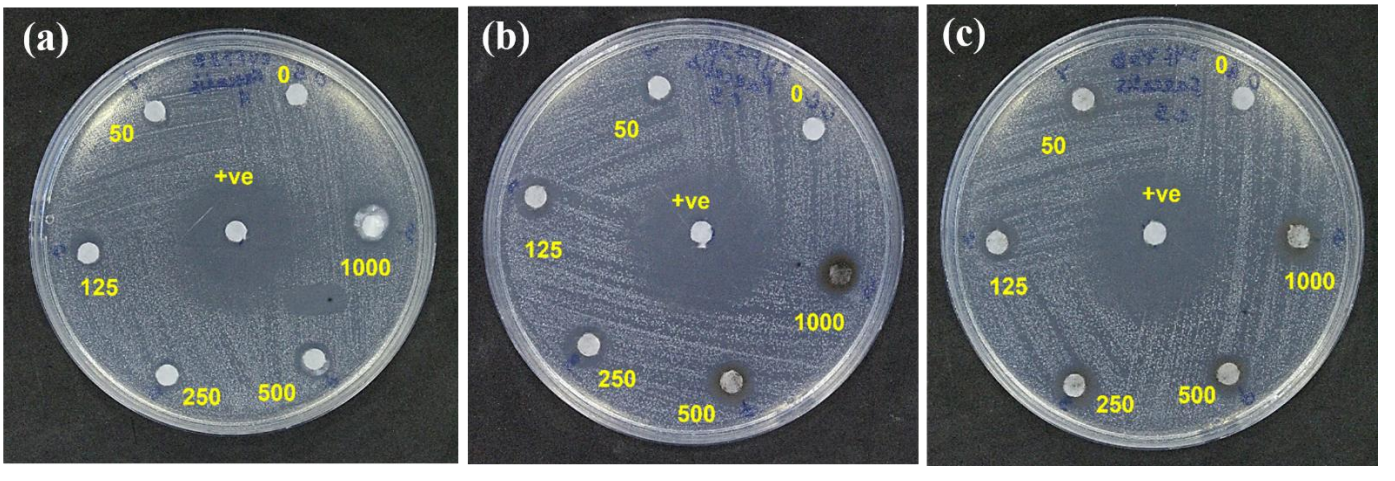

Fig. 5. (a-c) Zone of inhibition against *Enterococcus faecalis* **by** Biochar, Biochar/CuO and Biochar/CuO/BaO samples.

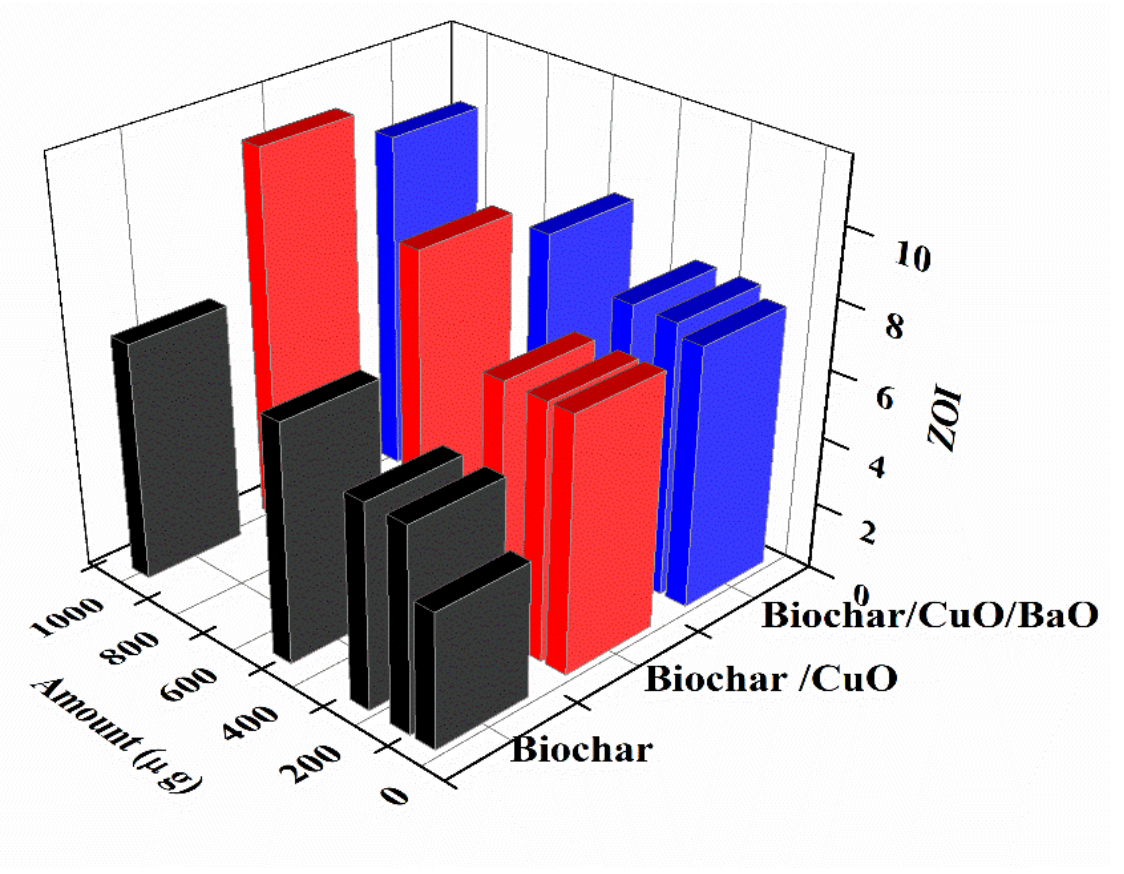

Fig. 6. Zone of inhibition against ***Enterococcus faecalis*** **by** Biochar, Biochar/CuO and Biochar/CuO/BaO samples at different concentrations.

The antibacterial efficacy of biochar-supported metal oxides like CuO and potentially BaO is attributed to several factors, including the physical disruption of bacterial membranes, the release of metal ions, and the production of ROS [28]. Additionally, CuO particles incorporation into biochar matrices can improve its stability and reusability, making it a promising candidate for long-term antibacterial applications [29].These mechanisms are particularly effective against Gram-positive bacteria such as *E. faecalis*, which are known for their robust cell wall structures [30,31].

3.6. Photocatalytic activity

The potential of biochar, CuO impregnated biochar and BC/CuO/BaO as photo catalyst was investigated for photocatalytic degradation of methylene blue under UV-Vis irradiation in presence of 10–20 µL of H_2O_2. The progress of the degradation study was monitored using the absorption spectrum of methylene blue at 664 nm, after regular intervals of every 10 min up to 60 min. The sample was kept under dark conditions for 90 min and were taken out after every 15 min. It was observed that the adsorption equilibrium was attained after 30 min followed by the proper adsorption of dye molecules. The addition of BaO in biochar along with CuO synergistically enhances degradation efficiency as compared to biochar and biochar/CuO which is in agreement with band gap values of these samples [32]. Along with this, photocatalytic activity is reliant upon factors such as size, morphology, and energy gap of photocatalyst. The smaller band gap of CuO and BaO impregnated biochar photocatalyst and enhanced oxygen vacancies facilitated adsorption of dyes on surface.

Table 3. Photocatalytic degradation of methylene blue by Biochar, Biochar/CuO and Biochar/CuO/BaO samples at different concentrations.

	% degradation		
Samples	**10 mg**	**20 mg**	**30 mg**
Biochar	45.8	59	64
Biochar/CuO	69.6	79.9	91
Biochar/CuO/BaO	72.5	81.8	98.82

As shown in Table 3 and Figure 7, the Biochar/CuO/BaO composite demonstrated superior photocatalytic performance in degrading a 20 ppm methylene blue solution under visible light, achieving 98.8% degradation within 60 minutes by using 30 mg of the photocatalyst.

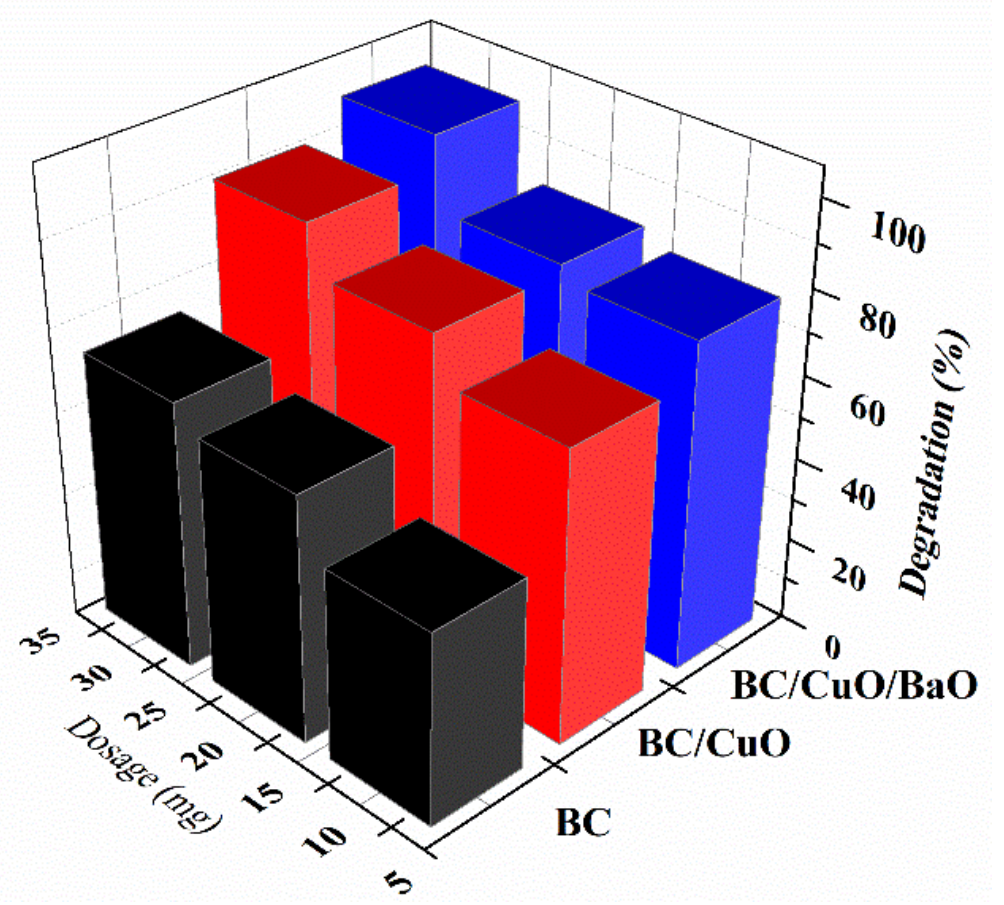

Fig. 7. Photocatalytic degradation of methylene blue by Biochar, Biochar/CuO and Biochar/CuO/BaO samples at different concentrations.

The enhanced efficiency is attributed to the synergistic effects of biochar's high surface area and the narrowed band gaps introduced by CuO and BaO, which improve visible light absorption and charge separation. These findings highlight the potential of biochar-based composites for sustainable wastewater treatment applications [33].

4. CONCLUSIONS

This research effectively illustrates the sustainable production of biochar-based nanocomposites, Biochar/CuO and Biochar/CuO/BaO, utilizing dead pine needles as a biomass precursor. The incorporation of CuO and BaO into the biochar matrix by a straightforward one-step pyrolysis technique markedly improved its structural, optical, and functional characteristics. Thorough characterization validated the crystalline integration of metal oxides, diminished bandgap energies, and enhanced surface morphology. The composites demonstrated outstanding photocatalytic efficacy in the degradation of methylene blue under visible light, with the Biochar/CuO/BaO composite attaining a degradation efficiency of up to 98.8%. The materials demonstrated significant antibacterial action, particularly against Enterococcus faecalis, confirming their potential for microbial control. The combined impacts of biochar's high porosity and the semiconductor characteristics of CuO and BaO enhance the functioning of these materials. This work emphasizes an environmentally sustainable and economically viable approach for transforming forest debris into value-added materials for wastewater treatment and biomedical uses, thereby advancing the concepts of circular economy and ecological sustainability.

DECLARATIONS

Ethical Approval

We affirm that this manuscript is an original work, has not been previously published, and is not currently under consideration for publication in any other journal or conference proceedings. All authors have reviewed and approved the manuscript, and the order of authorship has been mutually agreed upon.

Funding

Not applicable

Availability of data and material

All of the data obtained or analyzed during this study is included in the report that was submitted.

Conflicts of Interest

The authors declare that they have no financial or personal interests that could have influenced the research and findings presented in this paper. The authors alone are responsible for the content and writing of this article.

Authors' contributions

All authors contributed equally in the preparation of this manuscript.

REFERENCES

[1] Islam, T., Repon, M.R., Islam, T., Sarwar, Z. and Rahman, M.M., 2023. Impact of textile dyes on health and ecosystem: a review of structure, causes, and potential solutions. *Environmental Science and Pollution Research*, *30*(4), pp.9207-9242. https://doi.org/10.1007/s11356-022-24398-3.

[2] Oladoye, P.O., Ajiboye, T.O., Omotola, E.O. and Oyewola, O.J., 2022. Methylene blue dye: Toxicity and potential elimination technology from wastewater. *Results in Engineering*, *16*, p.100678. https://doi.org/10.1016/j.rineng.2022.100678.

[3] Yang, S., Meng, X., Zhen, Y., Baima, Q., Wang, Y., Jiang, X. and Xu, Z., 2024. Strategies and mechanisms targeting Enterococcus faecalis biofilms associated with endodontic infections: A comprehensive review. *Frontiers in Cellular and Infection Microbiology*, *14*, p.1433313. https://doi.org/10.3389/fcimb.2024.1433313.

[4] Ouyang, D., Chen, Y., Yan, J., Qian, L., Han, L. and Chen, M., 2019. Activation mechanism of peroxymonosulfate by biochar for catalytic degradation of 1, 4-dioxane: Important role of biochar defect structures. *Chemical Engineering Journal*, *370*, pp.614-624. https://doi.org/10.1016/j.cej.2019.03.235.

[5] Kalderis, D., Tsuchiya, S., Phillipou, K., Paschalidou, P., Pashalidis, I., Tashima, D. and Tsubota, T., 2020. Utilization of pine tree biochar produced by flame-curtain pyrolysis in two non-agricultural applications. *Bioresource Technology Reports*, *9*, p.100384. https://doi.org/10.1016/j.biteb.2020.100384.

[6] Alsukaibi, A.K., 2022. Various approaches for the detoxification of toxic dyes in wastewater. *Processes*, *10*(10), p.1968.https://doi.org/10.3390/pr10101968.

[7] Sharma, S., Chauhan, A., Ranjan, A., Mathkor, D.M., Haque, S., Ramniwas, S., Tuli, H.S., Jindal, T. and Yadav, V., 2024. Emerging challenges in antimicrobial resistance: implications for pathogenic microorganisms, novel antibiotics, and their impact on sustainability. *Frontiers in microbiology*, *15*, p.1403168. https://doi.org/10.3389/fmicb.2024.1403168.

[8] Zhao, C., Wang, B., Theng, B.K., Wu, P., Liu, F., Wang, S., Lee, X., Chen, M., Li, L. and Zhang, X., 2021. Formation and mechanisms of nano-metal oxide-biochar composites for pollutants removal: A review. *Science of the Total Environment*, *767*, p.145305. https://doi.org/10.1016/j.scitotenv.2021.145305.

[9] Zhu, Y., Yi, B., Yuan, Q., Wu, Y., Wang, M. and Yan, S., 2018. Removal of methylene blue from aqueous solution by cattle manure-derived low temperature biochar. *RSC advances*, *8*(36), pp.19917-19929. https://doi.org/10.1039/C8RA03018A.

[10] Gupta, A., Ghosh, P., Arora, K., Sharma, S. and Kumar, S., 2024. Valorization potential of pine needle waste biomass: recent trends and future perspectives. *Environmental Science and Pollution Research*, *31*(25), pp.36136-36151. https://doi.org/10.1007/s11356-023-27440-0.

[11] Gonçalves, N.P., Lourenço, M.A., Baleuri, S.R., Bianco, S., Jagdale, P. and Calza, P., 2022. Biochar waste-based ZnO materials as highly efficient photocatalysts for water treatment. *Journal of Environmental Chemical Engineering*, *10*(2), p.107256. https://doi.org/10.1016/j.jece.2022.107256.

[12] Thi Luyen, N., Van Nguyen, K., Van Dang, N., Quang Huy, T., Hoai Linh, P., Thanh Trung, N., Nguyen, V.T. and Thanh, D.V., 2023. Facile one-step pyrolysis of ZnO/biochar nanocomposite for highly efficient removal of methylene blue dye from aqueous solution. *ACS Omega*, *8*(30), pp.26816-26827. https://doi.org/10.1021/acsomega.3c01232.

[13] Hu, Z. and Wei, L., 2023. Review on characterization of biochar derived from biomass pyrolysis via reactive molecular dynamics simulations. *Journal of Composites Science*, *7*(9), p.354. https://doi.org/10.3390/jcs7090354.

[14] Kumar, R., Sharma, S., Kumari, N., Sharma, P., Sharma, N., Thakur, S., Sharma, R., Thakur, N. and Kumar, K., 2025. Biomass-Derived Biochar and CuO–NiO

Nanocomposites: Eco-Friendly Solutions for Environmental Cleanup. *International Journal of Environmental Research*, *19*(1), pp.1-22. https://doi.org/10.1007/s41742-024-00699-y.

[15] Sternig, A., Klacar, S., Bernardi, J., Stöger-Pollach, M., Gronbeck, H. and Diwald, O., 2011. Phase separation at the nanoscale: Structural properties of BaO segregates on MgO-based nanoparticles. *The Journal of Physical Chemistry C*, *115*(32), pp.15853-15861. https://doi.org/10.1021/jp204043g.

[16] Amin, F.R., Huang, Y., He, Y., Zhang, R., Liu, G. and Chen, C., 2016. Biochar applications and modern techniques for characterization. *Clean Technologies and Environmental Policy*, *18*, pp.1457-1473. https://doi.org/10.1007/s10098-016-1218-8.

[17] Radja, I., Yassin, M.T., Ezzat, A.O., AbdElkader, O.H., Benyoucef, A., Alkoudsi, B.D. and Sabantina, L., 2025. Construction of a ternary composite of mg-doped biochar/CuO, and PAni for supercapacitor applications. *Journal of Energy Storage*, *108*, p.114785. https://doi.org/10.1016/j.est.2024.114785.

[18] Islam, M.R., Sen, S.K., Kumar, A., Islam, M.S., Manir, M.S., Ara, Z., Hossain, M.D. and Alam, M.K., 2024. Effect of gamma (γ-) radiation on the opto-structural and morphological properties of green synthesized BaO nanoparticles using Moringa Oleifera leaves. *Heliyon*, *10*(4). https://doi.org/10.1016/j.heliyon.2024.e26350.

[19] Mian, M.M. and Liu, G., 2018. Recent progress in biochar-supported photocatalysts: synthesis, role of biochar, and applications. *RSC Advances*, *8*(26), pp.14237-14248. https://doi.org/10.1039/C8RA02258E.

[20] Khataee, A., Kalderis, D., Gholami, P., Fazli, A., Moschogiannaki, M., Binas, V., Lykaki, M. and Konsolakis, M., 2019. Cu_2O-CuO@ biochar composite: synthesis, characterization and its efficient photocatalytic performance. *Applied Surface Science*, *498*, p.143846. https://doi.org/10.1016/j.apsusc.2019.143846.

[21] Nazir, S., Zhang, J.M., Junaid, M., Saleem, S., Ali, A., Ullah, A. and Khan, S., 2024. Metal-based nanoparticles: basics, types, fabrications and their electronic applications. *Zeitschrift für Physikalische Chemie*, *238*(6), pp.965-995. https://doi.org/10.1166/mex.2023.2508.

[22] Wang, Q., Luo, B., Wang, Z., Hu, Y. and Du, M., 2024. Pore Engineering in Biomass-Derived Carbon Materials for Enhanced Energy, Catalysis, and Environmental Applications. *Molecules*, *29*(21), p.5172. https://doi.org/10.3390/molecules29215172.

[23] Imran, M., Ali, L., Ali, L., Wakeel, M., Siddique, M.H., Khan, Z.U.H., Murtaza, B., Iqbal, J., Al-Kahtani, A.A. and Shahid, M., 2023. Remediation potential of biochar/copper oxide nanoparticles composite for lead- and cadmium-contaminated wastewater. *Environmental Earth Sciences*, *82*(23), p.574. https://doi.org/10.1007/s12665-023-11147-z.

[24] Raj, R.B., Umadevi, M., Parimaladevi, R. and Anuratha, M., 2022. ZnO/BaO nanocomposites: a promising photocatalyst in degrading anionic and cationic dyes under UV and visible light and an efficient antibacterial agent. *Journal of Sol-Gel Science and Technology*, *102*(3), pp.628-636. https://doi.org/10.1007/s10971-021-05667-y.

[25] Shukla, S., Shukla, S.K., Singh, P., Pandey, H., Dikshit, A. and Pandey, A.C., 2025. Measurement of antibiotic removal efficiency of ZnO-WO3 nanocomposite and its validation through residual antimicrobial activity. *Heliyon*, *11*(2). p.e41816. https://doi.org/10.1016/j.heliyon.2025.e41816.

[26] Yang, B., Zhang, M., Wu, M., Zhang, H., Song, Q. and Yu, S., 2019. Synthesis of biochar-based Cu2O nanoparticles and their antibacterial activity against Escherichia coli. *Inorganic and Nano-Metal Chemistry*, *49*(1), pp.12-16. https://doi.org/10.1080/24701556.2019.1571512.

[27] Čech Barabaszová, K., Holešová, S., Bílý, M. and Hundáková, M., 2020. CuO and CuO/vermiculite based nanoparticles in antibacterial PVAc nanocomposites. *Journal of Inorganic and Organometallic Polymers and Materials*, *30*(10), pp.4218-4227. https://doi.org/10.1007/s10904-020-01573-y.

[28] Gu, H., Chen, X., Chen, F., Zhou, X. and Parsaee, Z., 2018. Ultrasound-assisted biosynthesis of CuO-NPs using brown alga Cystoseira trinodis: Characterization, photocatalytic AOP, DPPH scavenging and antibacterial investigations. *Ultrasonics Sonochemistry*, *41*, pp.109-119. https://doi.org/10.1016/j.ultsonch.2017.09.006.

[29] Cai, S., Liu, Y. and Chen, J., 2020. FeCu-biochar enhances the removal of antibacterial sulfapyridine from groundwater by activation of persulfate. *Environmental Chemistry Letters*, *18*, pp.1693-1700. https://doi.org/10.1007/s10311-020-01026-5.

[30] Kociołek-Balawejder, E., Stanisławska, E., Dworniczek, E., Seniuk, A., Jacukowicz-Sobala, I. and Winiarska, K., 2019. Cu_2O doped gel-type anion exchanger obtained by reduction of brochantite deposit and its antimicrobial activity. *Reactive and Functional Polymers*, *141*, pp.42-49. https://doi.org/10.1016/j.reactfunctpolym.2019.05.006.

[31] Keskin, N.B., Aydın, Z.U., Uslu, G., Özyürek, T., Erdönmez, D. and Gündoğar, M., 2021. Antibacterial efficacy of copper-added chitosan nanoparticles: A confocal laser scanning microscopy analysis. *Odontology*, *109*(4), pp.868-873. https://doi.org/10.1007/s10266-021-00613-4.

[32] Yu, F., Tian, F., Zou, H., Ye, Z., Peng, C., Huang, J.,

Zheng, Y., Zhang, Y., Yang, Y., Wei, X. and Gao, B., 2021. ZnO/biochar nanocomposites via solvent free ball milling for enhanced adsorption and photocatalytic degradation of methylene blue. *Journal of Hazardous Materials*, *415*, p.125511. https://doi.org/10.1016/j.jhazmat.2021.125511.

[33] Nogueira, A.C., Gomes, L.E., Ferencz, J.A., Rodrigues, J.E., Goncalves, R.V. and Wender, H., 2019. Improved visible light photoactivity of $CuBi_2O_4$/CuO heterojunctions for photodegradation of methylene blue and metronidazole. *The Journal of Physical Chemistry C*, *123*(42), pp.25680-25690. https://doi.org/10.1021/acs.jpcc.9b06907.

